HHS Public Access

Author manuscript

Exp Eye Res. Author manuscript; available in PMC 2016 March 01.

Published in final edited form as:

Exp Eye Res. 2015 March ; 132: 78–90. doi:10.1016/j.exer.2015.01.018.

Lipid Domains in Intact Fiber-Cell Plasma Membranes Isolated from Cortical and Nuclear Regions of Human Eye Lenses of Donors from Different Age Groups

Marija Raguz[a,c,1], **Laxman Mainali**[a,1], **William J. O'Brien**[b], and **Witold K. Subczynski**[a,*]

[a]Department of Biophysics, Medical College of Wisconsin, Milwaukee, WI 53226, USA

[b]Department of Ophthalmology, Medical College of Wisconsin, Milwaukee, WI 53226, USA

[c]Department of Medical Physics and Biophysics, School of Medicine, University of Split, Split, Croatia

Abstract

The results reported here clearly document changes in the properties and the organization of fiber-cell membrane lipids that occur with age, based on electron paramagnetic resonance (EPR) analysis of lens membranes of clear lenses from donors of age groups from 0 to 20, 21 to 40, and 61 to 80 years. The physical properties, including profiles of the alkyl chain order, fluidity, hydrophobicity, and oxygen transport parameter, were investigated using EPR spin-labeling methods, which also provide an opportunity to discriminate coexisting lipid domains and to evaluate the relative amounts of lipids in these domains. Fiber-cell membranes were found to contain three distinct lipid environments: bulk lipid domain, which appears minimally affected by membrane proteins, and two domains that appear due to the presence of membrane proteins, namely boundary and trapped lipid domains. In nuclear membranes the amount of boundary and trapped phospholipids as well as the amount of cholesterol in trapped lipid domains increased with the donors' age and was greater than that in cortical membranes. The difference between the amounts of lipids in domains uniquely formed due to the presence of membrane proteins in nuclear and cortical membranes increased with the donors' age. It was also shown that cholesterol was to a large degree excluded from trapped lipid domains in cortical membranes. It is evident that the rigidity of nuclear membranes was greater than that of cortical membranes for all age groups. The amount of lipids in domains of low oxygen permeability, mainly in trapped lipid domains, were greater in nuclear than cortical membranes and increased with the age of donors. These results indicate that the nuclear fiber cell plasma membranes were less permeable to oxygen than cortical membranes and become less permeable to oxygen with age. In clear lenses, age-related

*Corresponding Author: Witold K. Subczynski, Department of Biophysics, Medical College of Wisconsin, 8701 Watertown Plank Road, Milwaukee, WI 53226, USA. Tel: (414) 456-4038; Fax: (414) 456-6512; subczyn@mcw.edu.

[1]The first two authors contributed equally to this work.

changes in the lens lipid and protein composition and organization appear to occur in ways that increase fiber cell plasma membrane resistance to oxygen permeation.

Keywords

cholesterol; membrane domains; fluidity; hydrophobic barrier; oxygen permeation; spin labeling

1. Introduction

Fiber-cells, which form tightly packed layers in the eye lens, lose their organelles soon after they are formed (Bassnett et al., 2011; Rafferty, 1985; Wride, 2011); the plasma membrane becomes the only membranous structure of matured fiber-cells. The lipid bilayer portion of the membrane determines bulk membrane properties (including diffusion barriers) (Borchman and Yappert, 2010; Subczynski et al., 2012) and can affect the properties of membrane proteins (Epand, 2005; Gonen et al., 2005; Reichow and Gonen, 2009; Tong et al., 2012; Tong et al., 2013). Age-related changes in the plasma membranes of human eye lens fiber-cells are much greater than age related changes in the membranes of other organs and tissues. Phospholipid (PL) composition changes drastically with age, with the increase of sphingolipid content (Borchman et al., 1994; Deeley et al., 2008; Yappert and Borchman, 2004; Yappert et al., 2003) and depletion of phosphatidylcholine (Borchman et al., 1994; Deeley et al., 2008; Yappert and Borchman, 2004; Yappert et al., 2003). The saturation levels of PL alkyl chains also increase (Deeley et al., 2008; Li et al., 1985; Yappert et al., 2003). Most characteristic is the increase in cholesterol (Chol) content up to the Chol/PL ratio of 4 (Li et al., 1985, 1987; Rujoi et al., 2003; Zelenka, 1984; Mainali et al., 2015). Aged fiber-cell membranes are loaded with integral proteins (Bassnett et al., 2011; Gonen et al., 2004; Kistler and Bullivant, 1980), the organization of which, including the formation of domains, arrays, and other structures, also changes with age (Buzhynskyy et al., 2007; Costello et al., 1989; Dunia et al., 2006; Zampighi et al., 2002). Regardless of these changes, the lens normally remains transparent. Due to a lack of turnover (Lynnerup et al., 2008), cells in the center of the nucleus of an adult human lens are as old as the individual, and membrane proteins that perform several functions in young human lenses likely perform the same functions in older lenses with altered lipid compositions. Thus, homeostasis of the fiber-cell plasma membrane and fiber cell itself should be maintained throughout the entire human life. We believe that the fiber-cell plasma membrane, with its unique structure and properties, helps to maintain cell homeostasis.

Previously, we have investigated the organization, properties, and dynamics of eye lens lipid membranes made of total lipids extracted from eyes of different species, donors of different age, and different regions of the eye lens (Mainali et al., 2012, 2013b; Raguz et al., 2008, 2009; Widomska et al., 2007). These works were summarized in the review (Subczynski et al., 2012) where we identified the significant functions of Chol specific to the fiber-cell plasma membrane. In human fiber-cell plasma membranes, Chol not only saturates the bulk PL bilayer (Mainali et al., 2013b) but also induces formation of immiscible pure cholesterol bilayer domains (CBDs) within the membrane (Jacob et al., 1999; Mainali et al., 2013b). The saturating Chol content keeps the bulk physical properties of lens-lipid membranes

consistent and independent of changes in PL composition. Thus, the CBD helps to maintain lens membrane homeostasis by providing the buffering capacity for Chol concentration in the surrounding PL bilayer, keeping it at a constant saturation level. This is especially significant for human lenses because among mammalian lenses, those from humans have the longest life span, and changes in lens PL composition with age are most pronounced (Estrada et al., 2010). Other functions of Chol include the formation of a hydrophobic barrier and the alteration of membrane lipid rigidity (Subczynski et al., 1994).

Our most recent studies have focused on intact lens membranes isolated from human (Raguz et al., 2014) and porcine (Mainali et al., 2012) lenses. We hypothesized that we should find the presence of the four purported lipid domains, namely bulk, boundary, and trapped lipids, as well as the pure CBD. We were able to confirm the existence of three of them: bulk, boundary, and trapped lipid domains (Mainali et al., 2012; Raguz et al., 2014). CBDs have been observed in bilayers containing lipids isolated from fiber cells membranes (Mainali et al., 2013b), but have not been observed in intact membranes. We also made an effort to quantitatively evaluate the relative amounts of PLs and Chol in lipid domains in intact human eye lens membranes (Raguz et al., 2014). All of these measurements were obtained using samples pooled from about twenty clear lenses.

In the studies reported here, we have extended our work in order to study the properties of the lipid bilayer portion of the intact fiber-cell plasma membranes of donors in age groups ranged from 0 to 20, 21 to 40, and 61 to 80 years, which compliment those obtained earlier from donors of the age group from 41 to 60 years (Raguz et al., 2014). Results were obtained for cortical and nuclear intact membranes isolated from clear lenses in each age group, which has allowed us to assess changes in the organization of lipids that occur with age. The data indicate that the amount of lipids in domains uniquely formed due to the presence of integral membrane proteins is greater in nuclear membranes than in cortical membranes and in nuclear membranes increases significantly with age. These studies will guide future work in which we are planning to assess changes that occur during cataract formation.

2. Materials and Methods

2.1. Materials

Doxylstearic acid spin labels (*n*-SASL, *n* = 5, 7, 9, 12, or 16) and androstane spin label (ASL) (see Fig. 1 in (Raguz et al., 2014) for their structure) were purchased from Molecular Probes (Eugene, OR). Other chemicals of at least reagent grade were purchased from Sigma-Aldrich (St. Louis, MO).

2.2. Isolation of intact membranes from cortical and nuclear fiber cell membranes

Twenty clear human lenses from donors in each of three groups, ranging in age from 0 to 20 (average age of 17.5 years, 4 female, 16 male, and all Caucasian donors), 21 to 40 (average age of 30.8 years, 4 female, 16 male, 18 Caucasian, and 2 African American donors), and 61 to 80 years (average age of 67.4 years, 6 female, 14 male, 19 Caucasian, and 1 African American donor), were obtained from the Lions Eye Bank of Wisconsin. Separately, seven pairs of clear lenses from donors of different ages (all male and all Caucasian) were also

obtained from the same Eye Bank and were used for single donor and single lens measurements. Lenses were removed *in situ* from refrigerated bodies within an average time frame of nine hours postmortem. All of the lenses were stored at −80°C until intact membrane isolations were performed. Lenses were examined using a binocular microscope and were evaluated for color and opacities to determine the presence or absence of cataractous changes. Usually lenses were accumulated over four months, intact membrane isolations were then performed. The cortical and nuclear regions of these lenses were separated based on differences in tissue consistency (Estrada and Yappert, 2004; Rujoi et al., 2003). Cortical and nuclear intact membranes were isolated based on minor modifications of the method developed by Bloemendal et al. (1972), as reported earlier (Cenedella and Fleschner, 1992; Chandrasekher and Cenedella, 1995; Lim et al., 2005). Each time special care was taken to produce a uniform suspension by repeatedly aspirating the solution through a syringe fitted with an 18-gauge needle. Finally, the pellet was washed and re-suspended with buffer (0.1 M borate, pH 9.5) and stored at −20°C. The same preparation procedures were used for isolation of cortical and nuclear intact membranes from three pairs of lenses from three different donors and for isolation of cortical and nuclear intact membranes from left and right eye lenses from four different donors.

2.3. Preparation of samples for EPR measurements

Spin labeling of intact membranes using *n*-SASLs and ASL was performed as described earlier (Ligeza et al., 1998; Mainali et al., 2012). The film of *n*-SASL was prepared on the bottom of a test tube by drying the appropriate amount of spin label in chloroform (to achieve the molar ratio of spin label: total lipids of 1:100 in each sample). Only one type of spin label was present in each sample. Intact membrane suspensions (~0.2 mL) were added to the test tubes and shaken for about two hours at room temperature. Control measurements demonstrated that this incubation time was sufficient to incorporate nearly all of the spin labeled molecules into the membranes. Spin labeled membrane suspensions were centrifuged twice using an Eppendorf centrifuge (16,000 g, 20 min, 4°C), and each time the excess of supernatant was removed. The final loose pellet was transferred to a 0.6 mm i.d. capillary made of gas-permeable methylpentene polymer (TPX) and used for EPR measurements (Subczynski et al., 2005).

2.4. EPR measurements

Conventional EPR spectra were recorded with a Bruker EMX spectrometer equipped with temperature-control accessories. All spectra were obtained at 37°C. Details of measurements were the same as those described earlier (Mainali et al., 2012; Raguz et al., 2014). Samples were thoroughly deoxygenated, yielding correct EPR line shapes. Maximum splitting values were measured within the precision of ±0.5 G and ±1.0 G for fluid and immobilized components, respectively, in intact membranes. Values of $2A_Z$, determined from the EPR spectra for samples frozen at −165°C, were measured within the precision of ±1.0 G.

Saturation-recovery (SR) EPR signals were obtained at X-band on a home-built spectrometer and loop-gap resonator, as previously described (Yin and Subczynski, 1996). The central-field hyperfine line, which is the most intense, was observed. Spin-lattice relaxation times, T_1s, of spin labels were determined by analyzing the SR signal for

deoxygenated samples (Kawasaki et al., 2001; Subczynski et al., 1989; Yin and Subczynski, 1996). For measurements of the oxygen transport parameter (OTP), the sample was equilibrated with the same gas that was used for temperature control (*i.e.*, a controlled air/nitrogen mixture adjusted with flowmeters [Matheson Gas Products, model 7631H-604]) (Kusumi et al., 1982; Subczynski et al., 1992a), and SR signals were recorded. SR signals were fitted by single- or double-exponential functions. The uncertainties in the measurements of decay time from the fits were usually less than 0.05%, whereas the decay times determined from sample to sample were within a precision of ±3% when a single-exponential fit was satisfactory and within a precision of ±5% and ±10% for longer and shorter recovery time constants when a double-exponential fit was satisfactory.

2.5. Distribution of PLs (% of total PLs) and Chol (% of total Chol) between domains in intact membranes

Based on the EPR spectrum of the PL analog 12-SASL, which is a superposition of spectra coming from bulk PLs and from boundary plus trapped PLs, relative amounts of PLs in these domains were evaluated. The relative distribution of Chol was investigated based on the distribution of a Chol analog spin label, ASL. Similar evaluations, as for 12-SASL, were performed based on conventional EPR spectra of ASL in intact membranes. The precision of these evaluations was better than 5%, because a 5% change in the contribution of each component decreased the goodness of the fit. These procedures were successfully applied to intact human membranes pooled from approximately 20 clear lenses obtained from 41- to 60-year-old donors Raguz et al. (2014) and are described in detail in Sect. 3.3. Here, we applied these procedures for cortical and nuclear intact membranes isolated from a pool of 20 clear human lenses in each of three different age groups (0–20, 21–40, and 61–80 years old), intact membranes isolated from a pool of two lenses from single donors, and intact membranes separately isolated from left and right eye lenses of single donors. We compared results with those obtained previously from lenses of 41-to 60-year-old donors.

3. Results

3.1. Conventional EPR

Figure 1 shows representative EPR spectra of 12-SASL coming from cortical (A) and nuclear (B) intact membranes isolated from the youngest investigated age group of 0- to 20-year-old donors. These spectra are compared with those that came from cortical (C) and nuclear (D) intact membranes from the oldest group, 61- to 80-year-old donors. All spectra show the presence of the strongly (component 1) and the weakly (component 2) immobilized component. The small, sharp component 3 comes from the very small amount of free 12-SASL remaining in the buffer. This component does not interfere with our measurements of the maximum splitting in strongly and weakly immobilized components, and can be subtracted from the superimposed EPR spectrum if necessary. Based on the qualitative analysis of spectra presented in Fig. 1, two major conclusions can be made. The amount of the strongly immobilized component (component 1) was greater in nuclear membranes than in cortical membranes in both age groups. It is also clear that the amount of strongly immobilized component was greater in membranes from the oldest donors (61–80 years old) compared to donors from 0–20 years of age. As indicated in Mainali et al., (2012)

and Raguz et al., (2014), the weakly immobilized component comes from bulk lipids and the strongly immobilized component from boundary plus trapped lipids. The results from the quantitative evaluation of the amount of PLs in the identified membrane domains are presented in Sect. 3.3.

EPR spectra coming from the Chol analog spin label ASL are shown in Fig. 2. Spectra from cortical (A) and nuclear (B) intact membranes isolated from the youngest investigated age group of 0- to 20-year-old donors are compared with those coming from cortical (C) and nuclear (D) intact membranes from the oldest group of 61- to 80-year-old donors. These spectra show distribution of Chol molecules between membrane domains. EPR spectrum of ASL coming from cortical membranes shows only the weakly immobilized component (component 2). This phenomenon was repeatedly observed in porcine intact membranes (Mainali et al., 2012) and in human intact membranes from donors of age groups of 0–20 (Fig. 2A), 21–40 (spectra not shown), and 41–60 (Raguz et al., 2014). EPR spectrum from cortical membranes of 61- to 80-year-old donors contains both weakly (component 2) and strongly (component 1) immobilized components (Fig. 2C). As shown in Fig. 2B and D, spectra from nuclear membranes of 0–20 and 61–80 year old donors are superimposed spectra from weakly and strongly immobilized components. Similar superimposed spectra were observed for nuclear membranes of 21–40 year old donors (spectra not shown) and 41–60 year old donors (Raguz et al., 2014). As indicated in Raguz et al. (2014), the weakly immobilized component came from ASL located in bulk lipids and in the CBD, while the strongly immobilized component came from ASL located in trapped lipids. Although we were unable to identify the CBD in intact membranes, (Mainali et al., 2012; Raguz et al., 2014) the conventional EPR spectra coming from Chol analog spin labels in the CBD and in the surrounding PL bilayer saturated with Chol were practically identical (Raguz et al., 2011a, b). Additionally, we should note that Chol molecules, as well as ASL, were substantially excluded from boundary lipids (Bieri and Wallach, 1975; Warren et al., 1975). Qualitative analysis of these spectra allows us to indicate that in cortical membranes the amount of Chol in trapped lipids was negligible (undetectable using conventional EPR approach) up to a certain donor age (~60 years). We can also conclude that the amount of Chol in nuclear membranes increases with age (see quantitative analysis in Sect. 3.3).

3.2. Saturation-recovery EPR

As indicated by residuals (the experimental signal minus the fitted curve) SR EPR signals from all spin labels used in the studies of intact lens membranes and obtained for deoxygenated samples can be successfully fitted only to the double-exponential functions. This observation indicates that spin labels are located in a minimum of two environments (membrane domains) with different fluidities in which the rotational motion of spin labels is significantly different. In deoxygenated samples, the rotational motion is the major factor that affects the spin-lattice relaxation rate (T_1^{-1}) of spin labels (Mailer et al., 2005; Robinson et al., 1994), and two values of T_1^{-1} extracted from the double exponential SR signals characterize spin label motion in two different domains. However, when the exchange rate of lipids (spin labels) between coexisting domains is greater than the T_1^{-1}, we measure an averaged T_1^{-1}, and domains cannot be discriminated using SR approach. This is the case for the coexisting bulk and boundary domains for which the exchange rate of lipids is ~10^7 s^{-1}

(Ryba et al., 1987; Ashikawa et al., 1994). The spin-lattice relaxation times for lipid spin labels in membranes lie between 1 and 10 μs (T_1^{-1} between 10^5 and 10^6 s^{-1}), and the SR approach recognizes these two domains as one, the bulk plus boundary domain.

SR signals from 12-SASL in Fig. 3 are good examples that show the abilities of the SR approach. Signals that come from cortical and nuclear membranes of 0–20 year old donors are presented in Fig. 3A and B, and those coming from 61–80 year old donors are presented in Fig. 3C and D. As indicated by residuals, for all signals fitting the experimental data to single-exponential modes were unsatisfactory, while double-exponential fits were excellent (additional criteria for the goodness of a single-exponential or a double-exponential fit are described in Subczynski et al., (2007)). The fast relaxation rate component was assigned to the bulk plus boundary lipids and the slow relaxation rate to the trapped lipids. Details for this assignment were described in Raguz et al. (2014).

Similarly, SR signals from Chol analog ASL were successfully fitted only by double exponentials (Fig. 4). Components in SR signals observed for all samples were assigned to ASL located in the boundary plus the CBD averaged environment (fast relaxation rate) and ASL located in trapped lipids (slow relaxation rate) (see also explanation in Sect. 3.1 and in Raguz et al. (2014)).

3.3. Distribution of PLs and Chol between domains in intact membranes from donors of different age groups

As follows from our paper (Raguz et al., 2014), 12-SASL (PL analogue spin label) is the best spin label to show the distribution of PLs between membrane domains discriminated in intact membranes. Conventional EPR spectra of 12-SASL (Fig. 1), which are the superposition of the spectrum coming from bulk PLs (weakly immobilized component) and the spectrum coming from boundary plus trapped PLs (strongly immobilized component), can be deconvoluted, giving the contribution of each component to the superimposed spectra. This procedure is shown in Fig. 5A for EPR spectrum of 12-SASL in nuclear intact membranes from clear human lenses of 61 to 80 year old donors. The EPR spectrum of 12-SASL in nuclear intact membranes (a) and the EPR spectrum of 12-SASL in nuclear lens lipid membranes (b) ((b) is a bulk component in spectrum (a)) are experimental spectra. The spectrum (c) is also the experimental spectrum of 12-SASL in the nuclear lens lipid membrane obtained at decreased temperature to get the spectrum with the same maximum splitting as that for the strongly immobilized component in spectrum (a) (value taken from Fig. 7D). The spectrum (c) should approximate the spectrum coming from the boundary plus trapped PLs with the motion decreased to almost rigid limit conditions. The spectrum (a) can be successfully reproduced by adding 44% of spectrum (b) and 56% of spectrum (c), where 100% of spectrum (b) and (c) indicates spectra with the same intensity (the same surface under the absorption curve). Similar procedures were performed for cortical and nuclear membranes isolated from a pool of 20 clear human lenses in each of three different age groups (0–20, 21–40, and 61–80 years old), membranes isolated from a pool of 2 lenses from single donors, and membranes separately isolated from left and right eye lenses of single donors.

The relative distribution of Chol was indicated by the distribution of Chol analog, ASL. Similar evaluations, as illustrated in Fig, 5A can be performed based on conventional EPR spectra of ASL in intact membranes (Fig. 2). The procedure is shown in Fig. 5B for EPR spectrum of ASL in nuclear intact membranes from clear human lenses of 61 to 80 year old donors. The assignment of the weakly immobilized component to Chol in the bulk domain and the strongly immobilized component to Chol in the trapped lipid domain is explained in Sect. 3.1.

Figure 6 summarizes the quantitative evaluations of the relative amounts of PLs and Chol in lipid domains of intact human eye lens membranes as a function of the age of donors. Results are presented for cortical and nuclear membranes isolated from a pool of 20 clear human lenses in each of three different age groups (0–20, 21–40, and 61–80 years old) investigated in the presented work. Recently published results for the age group of 41 to 60-year old donors are also included in Fig. 6. Based on conventional EPR spectra of 12-SASL (PL analog spin label), such as those presented in Fig. 1 and on the procedure description in Fig. 5A, we evaluated the amount of PLs in domains formed due to the presence of integral membrane proteins, namely in boundary plus trapped lipid domains (Fig. 6A). The amount of PLs in boundary plus trapped lipid domains increased with age from 36% (0- to 20-year-old donors) to 56% (61- to 80-year-old donors) for nuclear membranes and from 28% (0- to 20-year-old donors) to 37% (41- to 60-year-old donors) and 35% (61- to 80-year-old donors) for cortical membranes. The amount of PLs in boundary and trapped lipid domains was greater in nuclear than in cortical membranes for all age groups, and this difference increased with age.

Figure 6 also contains quantitative data about the distribution of Chol between membrane domains which were obtained with the Chol analog spin label ASL. As indicated in Sect. 3.1, conventional EPR spectra of ASL discriminated ASL located in the bulk domain (and the CBD – purported domain which was not yet identified in intact membranes) and in the trapped lipid domain. Chol and ASL were substantially excluded from the boundary lipid domain. Results presented in Fig. 6B were based on conventional EPR spectra of ASL (as those presented in Fig. 2) and on the procedure description in Fig. 5B. They showed almost four fold increase of Chol content in trapped lipids in nuclear membranes between the youngest and the oldest investigated age group. Surprisingly, this approach did not detect Chol in trapped lipids in cortical membranes. A small amount (~5% from total Chol) was detected only for the oldest age group (61- to 80-year-old donors).

To finish all measurements with all steraic acid and Chol analog spin labels and using the existing X-band EPR spin-labeling approaches, we prepared samples (cortical and nuclear intact membranes) from ~20 pooled lenses. In addition to the methodological benefits (handling the sample, good signal-to-noise ratio), mixing the samples from 20 lenses enabled us to obtain averaged information about the organization of lipids in membranes from different age groups. Most significantly, it allowed the assessment of a major tendency for organizational changes that occurs with age. However, only one pool of membranes for each age group was studied in the present work, thus statistical variability could not be measured. To ensure that the changes we observed with pooled lenses were age-dependent, we performed measurements with single donor and single lens samples. Because of the

limited amount of membranes isolated from these lenses and the use of the X-band spectrometer with a loop-gap resonator that has a sample volume of 3 μL, we limited our measurements only to two spin labels. We chose 12-SASL and ASL which not only allowed us to confirm validity of the data about amounts of PLs and Chol in domains uniquely formed due to the presence of membrane proteins but also strengthened major conclusions about the changes in the amount of these lipids occurring with age, the number one risk factor associated with cataract. The data obtained are included as appropriate points in Fig. 6. These points are condensed within two donor age groups, from 15- to 27-year-old donors and from 53- to 67-year-old donors which allowed confirming major tendencies in organizational changes of intact cortical and nuclear membranes that occur with age as observed for pooled samples. Statistical analysis was performed and statistically significant differences were evaluated.

The quantitative data (mean values and standard deviations) of the relative amounts of PLs and Chol in lipid domains in intact lens membranes uniquely formed to the presence of membrane proteins obtained for different preparations of cortical and nuclear membranes from pairs of eye lenses from three different donors and eight lenses from four different donors are presented in Table 1. Measurements for single donor and single lens samples allowed us to determine *P* values using Student's t-test for differences between amounts of lipids in domains in lenses of old and young donors. These *P* values are included in Table 1. Statistically significant differences were confirmed. Thus our conclusions made based on the measurements from one pool (twenty lenses) of membranes for each age group remains. In nuclear membranes the amount of lipids in domains created due to the presence of membrane proteins at the donor age of 60.5 was greater than that at age of 20.6 ($P < 0.001$ for PL and $P < 0.001$ for Chol). In cortical membranes the amount of lipids in domains created due to the presence of membrane proteins at the donor age of 60.5 was greater than that at age of 20.6 with $P = 0.41$ for PL and $P = 0.04$ for Chol. We can conclude that these changes in cortical membranes were minimal, however, for Chol statistically significant. The data also indicate that at the donor age of 20.6 the amount of lipids in these domains in nuclear membranes was greater that that in cortical membranes ($P = 0.054$ for PL and $P < 0.001$ for Chol). At the donor age of 60.5 this difference was significantly greater ($P < 0.001$ for PL and $P < 0.001$ for Chol). The data presented in the Table 1 also confirmed that the increase of this difference with age of donor was statistically significant ($P < 0.001$ for PL and $P < 0.001$ for Chol).

3.4. Profiles of physical properties across domains in intact membranes

EPR spin-labeling methods provide a number of unique approaches for determining several important membrane properties as a function of bilayer depth. They include parameters that describe order and rotational motion of alkyl chains as well as parameters that describe bulk membrane properties, such as diffusion-concentration products for oxygen and hydrophobicity. These properties can be obtained for homogenous membranes and, in some cases, for coexisting membrane domains or coexisting membrane phases, without the need for their physical separation. In these studies, PL- and Chol analog spin labels were incorporated into the membrane with the nitroxide moiety, which gives rise to the observed EPR signal, at specific depths and in specific membrane domains. The physical/chemical

properties of the microenvironment in the immediate vicinity of the nitroxide were then characterized using EPR spectroscopic methods.

Figure 7 shows profiles across domains in intact human lens membranes from donors of different age groups obtained using EPR spin-labeling methods. Profiles describing order and rotational motion of alkyl chains are presented in Fig. 7A and B. Profiles describing bulk membrane properties, such as diffusion-concentration products for oxygen and hydrophobicity, are presented in Fig. 7C and D. Figure 7A, B, and C contain profiles across coexisting membrane domains.

3.4.1. Maximum splitting (alkyl chain order and fluidity)—The maximum splitting is a convenient spectral parameter that reports membrane fluidity at a certain depth when EPR spectra coming from *n*-SASLs in different membrane domains are overlapped (Fig. 7A). Smaller maximum-splitting values indicate greater membrane fluidity. This display additionally allowed discrimination of membrane domains as indicated by data of 12- and 16-SASL which clearly show weakly and strongly immobilized components. Profiles across more fluid domains were very similar to those of lens lipid membranes (Mainali et al., 2013b) and were assigned to bulk lipid domains, which were not affected by membrane integral proteins. Remaining profiles of strongly immobilized lipids, formed as a result of their interaction with integral membrane proteins, were assigned to boundary plus trapped lipid domains (see Mainali et al. (2012); Raguz et al., (2014) for more details).

The presence of proteins in intact membranes induced formation of a new lipid domain that is manifested by the presence of the strongly immobilized signal in EPR spectra of *n*-SASLs (component 1 in Fig. 1) in addition to the weekly immobilized signal typical for 12- and 16-SASL in lens lipid membranes (component 2 in Fig. 1). Maximum splitting values measured for 12- and 16-SASL in the most immobilized lipid domain were close to the rigid limit values for these spin labels (compare values in Fig. 7A with those in Fig. 7D, remembering that the rigid limit value is the $2A_Z$ value). Thus, the alkyl chains in these domains were practically immobile in the membrane center. The bell-shaped profiles of membrane fluidity in these domains were inverted as compared to profiles in bulk lipids. All of these indicate that alkyl chains were strongly immobilized by the contact with membrane proteins. Interestingly, membrane fluidity in the bulk domain increased toward the membrane center while, in the remaining domains, the membrane fluidity decreased toward the membrane center. These features were observed in cortical and nuclear membranes in all investigated age groups. This display of membrane fluidity shows no differences between age groups. Values measured in bulk lipids were the same, which is in agreement with data for lens lipid membranes and additionally confirms that profiles of membrane fluidity do not depend on PL composition when membranes are saturated with Chol (Subczynski et al., 2012). For all age groups, profiles across boundary plus trapped lipid domains in the cortical membranes were nearly the same as profiles in the nuclear membranes, within the limit of the experimental uncertainty.

3.4.2. Spin-lattice relaxation rate (alkyl chain fluidity)—The spin-lattice relaxation rate (T_1^{-1}), obtained from SR EPR of *n*-SASLs in deoxygenated samples (Fig. 3) depends primarily on the rotational motion of the nitroxide moiety within the lipid bilayer (Mailer et

al., 2005; Robinson et al., 1994). Hence, T_1^{-1} can be used as a convenient quantitative measure of membrane fluidity (Mainali et al., 2011a; Mainali et al., 2013a). The fluidity in this display (Fig. 7B) reflects the rate of motion of this fragment of the alkyl chain of the PL to which the nitroxide moiety is rigidly attached. High fluidity profiles were assigned to PLs in the bulk plus boundary domain (the lipid exchange rate between these domains is faster than T_1^{-1}). Remaining profiles with low T_1^{-1} were assigned to trapped lipids (see (Raguz et al., 2014) for more details). The bulk plus boundary domain and the trapped lipid domain can be discriminated with this method by all *n*-SASLs, giving additional information about depth dependence dynamics of alkyl chains of PLs in each domain without their physical separation. As indicated by points for T_1^{-1} obtained from SR EPR of ASL in deoxygenated samples (Fig. 4), also ASL can discriminate these domains (Fig. 7B).

Based on the data presented in Fig. 7B profiles, two conclusions can be drawn that are valid for all investigated age groups. (1) Alkyl chains are very immobile in the trapped lipids, and membrane dynamics are suppressed in these domains to the level of gel-phase. (2) Because the trapped lipid domain was discriminated from the bulk plus boundary domains using the T_1-sensitive method, the lipid exchange rate between discriminated domains has to be smaller than the smallest spin-lattice relaxation rate of spin labels, which is 0.2×10^6 s^{-1} for the trapped lipids.

3.4.3. Oxygen transport parameter (membrane fluidity)—Membrane fluidity can not only be studied by measuring the maximum splitting or the spin-lattice relaxation rate, each of which reflect the order and/or dynamics of alkyl chains, but also by monitoring the motion of molecular oxygen within the membrane. In this SR EPR method, the measured value is the bimolecular collision rate between oxygen and the nitroxide moiety of spin labels expressed as the OTP (Kusumi et al., 1982; Subczynski et al., 2007). This method is extremely sensitive to changes in the local oxygen diffusion-concentration product around the nitroxide moiety. SR signals obtained in the presence of oxygen for all spin labels in cortical and nuclear membranes can be fitted satisfactory only with double-exponential functions (data not shown). This indicates that spin labels are located in two environments with different fluidity (as indicated in Sect. 3.2) but also with different OTP. Profiles with higher OTP (Fig. 7C) were assigned to the bulk plus boundary domain (see (Ashikawa et al., 1994)), and remaining profiles were assigned to trapped lipids. Based on profiles of the OTP across membrane domains, and using procedures described in Subczynski et al. (1989), permeability coefficients for oxygen across these domains can be evaluated. Because the OTP was measured only in the hydrocarbon region of the lipid bilayer portion of the intact membranes, the permeability coefficients for oxygen (P_M) were estimated only across the hydrocarbon regions of the discriminated domains and are collected in Table 2.

Values of the OTP obtained with the Chol analog spin label, ASL, were included into profiles in Fig. 7C at appropriate depth. ASL also discriminates two domains in intact membranes, giving two values of the OTP. Values measured in more fluid domains were significantly larger than those measured with *n*-SASL, although they were still considerably smaller than those measured with ASL in lens lipid membranes (Mainali et al., 2013b). The reasonable explanation for this is that ASL is excluded from boundary lipids, and the OTP is not affected by the boundary lipid domain, as in the case of *n*-SASLs. Values measured in

less fluid domains fall into profiles across trapped lipid domains. Results presented in Sect. 3.2 ensure that these values described oxygen movement within the trapped lipids and not within the CBD. Although ASL discriminates the CBD in cortical and nuclear lens lipid membranes (Mainali et al., 2011b; Mainali et al., 2012, 2013b; Raguz et al., 2008, 2009), we have not yet been able to discriminate the CBD in intact membranes (Mainali et al., 2012).

3.4.4. $2A_Z$ values (membrane hydrophobicity)—Figure 7D shows hydrophobicity profiles across the lipid bilayer portion of intact lens membranes. In these profiles, $2A_Z$ values (z-component of the hyperfine-interaction tensor) are plotted as a function of membrane depth. Smaller $2A_Z$ values indicate higher hydrophobicity. The local hydrophobicity, as observed by $2A_Z$, can be related to the hydrophobicity (or ε) of an organic solvent (Subczynski et al., 1994). All profiles in Fig. 7D indicate the existence of a high hydrophobic barrier in the center of intact membranes with hydrophobicity comparable to that of N-butylamine and 1-decanol ($\varepsilon = 6–8$), which ensures that the transport of water, ions, and other small polar and ionic molecules is tightly controlled by membrane proteins.

The presence of proteins changes rectangular hydrophobicity profiles, as observed for lens lipid membranes (Mainali et al., 2012, 2013b; Raguz et al., 2008, 2009; Widomska et al., 2007), to bell-shaped profiles. The center of intact membranes becomes less hydrophobic than the center of lens lipid membranes. Although, it still forms a considerably high hydrophobic barrier to protect uncontrolled leakage of small polar molecules across fiber cell plasma membranes. The effect of membrane proteins on hydrophobicity profiles close to the membrane surface was rather negligible. Because $2A_Z$ values were measured for frozen membrane suspensions, the EPR spectrum is the superposition of individual spectra from all domains reporting averaged membrane hydrophobicity.

4. Discussion

The main goal of this research was to better understand the role of the lipid bilayer portion of the fiber-cell plasma membranes in maintaining lens transparency during the aging process. The lens is avascular, and because of that nutrients, including oxygen, must come to the lens interior through the diffusion process. To reach the lens center nutrients must pass thousands of fiber cell membranes, which form the only supramolecular structures of matured fiber cells (Beebe, 2003). There is a major difference between the transport of oxygen and other nutrients (which are mainly water soluble small molecular weight compounds) to the lens interior. Transport of water, ions, and other small polar and ionic molecules across fiber cell membranes (from fiber cell to fiber cell) is tightly controlled by membrane proteins. The most abundant integral transmembrane proteins in human lens fiber cell membranes which regulate communication between fiber cells are aquaporin-0 (AQP0) and connexins (Cx46 and Cx50) (Bassnett et al., 2011; Gonen et al., 2005; Reichow and Gonen, 2009). AQP0 belongs to the water transport family of integral channel proteins controling transport of water and some neutral solutes but not ions (Agre, 2004). Connexins, Cx46 and Cx50 (with Cx46 found mainly in the cortex and outer nuclear layers, and Cx50 found mainly in the nuclear core (Chung et al., 2007; Tenbroek et al., 1992; White et al., 1998)), form gap junctions between lens fiber cells and control the exchange of ions and small metabolites (glucose, amino acids) between lens cells (Mathias et al., 2010). Our

results indicate that for human clear lenses the lipid bilayer portion of fiber cell membranes forms a highly hydrophobic barrier in both cortical and nuclear membranes for all investigated age groups (Fig. 7D). We can conclude that the changes in the lipid composition that take place during the aging of fiber cells do not affect the membrane proteins' tight control of the transport of polar molecules from cell to cell, helping to maintain the cell and lens homeostasis.

Human eye-lens membranes are loaded with membrane integral proteins. Our results and published biochemical data suggest that both, the amount of protein and the packing of protein in membranes may be important in modifying the observed physical properties of the lipid bilayer and the distribution of lipids between membrane domains. Formation of boundary and/or trapped lipids is likely induced by the most abundant proteins in the human lens fiber cell membrane, namely AQP0 and connexins. These proteins form ordered two-dimensional arrays in fiber cell membranes (Buzhynskyy et al., 2007, 2011; Costello et al., 1989; Dunia et al., 2006; Gonen et al., 2004; Zampighi et al., 2002) and lipids can be trapped within these protein-dense structures. The density/distribution of these proteins varies with fiber cell age (Kuszak et al., 2004). For example the ordered arrays of AQP0 are enriched in the nucleus (Costello et al., 1989). These published data are in agreement with the results presented here which show that the amount of trapped lipids increased with the age of donor and is greater in the nucleus than in the cortex. The unexpected distribution of Chol between domains in cortical membranes which we observed can, to a certain degree, be explained not only by Chol substantial exclusion from boundary lipids (Bieri and Wallach, 1975; Warren et al., 1975), but also by the significant structural remodeling of gap junctions that takes place during fiber cell development and maturation (Biswas et al., 2009, 2010; Biswas and Lo, 2007). The newly formed gap junction channels in the superficial young fiber cells are continuously clustered, forming large Chol-rich loosely-packed gap junction plagues. In the matured inner cortical fibers they are transformed into Chol-free tightly-packed clusters. This observation suggests that in cortical membranes the amount of Chol in trapped lipid domains is low; close to zero as observed using conventional EPR approach.

To maintain lens transparency oxygen concentration in the lens should be very low, reaching a value close to zero in the lens nucleus (Eaton, 1991; Harding, 1991; McNulty et al., 2004). Factors that can cause cataract formation, including age (Bron et al., 2000; Truscott, 2005), hyperbaric oxygen treatment (Borchman et al., 2000; Freel et al., 2003; Huang et al., 2006; Huang et al., 2008; Palmquist et al., 1984), and vitrectomy (Chung et al., 2001; Harocopos et al., 2004; Hsuan et al., 2001), are directly related to the increased oxygen concentration within the lens interior. Thus, understanding the processes that control oxygen transport, concentration, and distribution in the lens are very important. Oxygen consumption is necessary to maintain a low oxygen concentration inside the eye lens; otherwise the concentration of oxygen would be equal to that outside the lens (Beebe et al., 2014; Siegfried et al., 2010). Mitochondrial respiration occurring in the outer layers of cortical fiber cells (not yet mature and containing organelles, including mitochondria) accounts for approximately 90% of oxygen consumption by the lens (McNulty et al., 2004), ensuring a low oxygen concentration in the lens nucleus. A high barrier to oxygen permeation located at the fiber-cell plasma membrane should help to keep oxygen concentration within the eye

lens at a very low level. This is especially important for the lens nucleus. A high barrier to oxygen permeation can help lower oxygen partial pressure in this region to below that in the cortex if a system to remove oxygen from the nucleus exists. This system should depend on non-mitochondrial oxygen consumption and be formed by ascorbate- (Eaton, 1991; McNulty et al., 2004) or glutathione-dependent oxygen consumption reactions (Beebe et al., 2011). High barriers to oxygen transport formed by the membranes of nuclear fiber cells can help to maintain a low oxygen partial pressure in the lens nucleus even at a very low oxygen consumption rate. It should be stressed that oxygen must pass through thousands of fiber-cell membranes on its way from the lens surface to its center, and a very small oxygen concentration difference across each membrane can significantly contribute to the oxygen concentration gradient across the eye lens.

Results presented in Table 2 indicate that for all membrane domains in cortical and nuclear fiber cell membranes, the permeability for oxygen was significantly lower than across water layers of the same thickness as these domains. Comparison of these data with oxygen permeability coefficients across lens lipid membranes (Mainali et al., 2013b) allowed us to conclude that the lowering effect was mainly due to the presence of membrane proteins and formation of boundary and trapped lipid domains. Interestingly, for all investigated age groups, the oxygen permeability coefficient across the bulk plus boundary domain was always smaller (in average by 30%) in nuclear membranes than in cortical. This difference was even greater for trapped lipids where the oxygen permeability coefficient across trapped lipids in nuclear membranes was in average smaller by 45%, compared to that in cortical membranes. Permeability of the trapped lipid domain in cortical and nuclear membranes was ~4.7 and ~8.5 times smaller, respectively, than the permeability across water layers of the same thickness as the domain. Thus, the trapped lipid domain formed a major membrane barrier for oxygen transport into the lens center, and this barrier was significantly greater in the lens nucleus. However, for all investigated age groups, values of the P_M measured for corresponding membrane domains do not change significantly with age.

The effective oxygen permeability coefficient across the lipid bilayer portion of the fiber cell plasma membrane is, in the first approximation, equal to the weighted sum of oxygen permeability coefficients evaluated for each lipid domain. The weight for each domain is proportional to the surface area occupied by the domain and to the total surface occupied by the lipid bilayer portion of the membrane. Values of the oxygen permeability coefficients across domains are listed in Table 2 and the relative amount of lipids (PLs and Chol), which determines the surface of the domain, is presented in Fig. 6. Our approaches indicate that the relative amounts of boundary and trapped PLs and trapped Chol in nuclear membranes increased significantly when the donor age increased (from the group of 0- to 20-year-old donors to the group of 61- to 80-year-old donors). The amount of lipids in those domains in cortical membranes did not change significantly with age. The combination of results presented in Table 2 and Fig. 6 allowed us to conclude that the high barrier to oxygen permeation into the lens center was formed by trapped lipids in the lipid bilayer portion of nuclear fiber cell membranes, and this barrier increased with the human age. In cortical fiber cell membranes barriers formed by the lipid bilayer domains were significantly lower than in

nuclear fiber cells and did not change with age, although these barriers were still considerably greater than across a water layer of the same thickness as domains.

Proteins are nearly impermeable to oxygen (Altenbach et al., 1994; Subczynski et al., 1992b). Thus, the total effective oxygen permeability coefficient across the intact fiber cell plasma membrane is equal to the oxygen permeability coefficient evaluated for the lipid bilayer portion of the membrane, multiplied by the factor proportional to the surface area of the lipid bilayer portion, divided by the surface area of the entire membrane. Because the protein content in human lens membranes is extremely high (Bassnett et al., 2011; Gonen et al., 2004; Kistler and Bullivant, 1980; Li et al., 1986; Li et al., 1985), it should significantly increase the total barrier properties of fiber cell intact membranes as compared with the barrier created only by the lipid bilayer portion of the membrane. The protein content increases with age (Bassnett et al., 2011; Gonen et al., 2004; Kistler and Bullivant, 1980) and is higher in the nucleus compared to content in the cortex (Li et al., 1986; Li et al., 1985), thus, the total barrier properties of fiber cell intact membranes are greater in aged fiber cells and in nuclear membranes than in cortical membranes. Our data strongly suggest that fiber cell plasma membranes form significant barriers to oxygen transport. Additionally, the data indicate that with age, the fiber cell plasma membrane becomes less permeable to oxygen. In clear lenses age-related changes in the lens lipid and protein composition and organization are orchestrated in a way that increases the fiber cell plasma membrane's resistance to oxygen permeation helping to maintain lens transparency and protecting against cataract formation.

Acknowledgments

This work was supported by grants EY015526, EB002052, EB001980, and EY001931 from the National Institutes of Health. Ivana Krpan assisted during sample preparations and EPR measurements.

References

Agre P. Nobel Lecture. Aquaporin water channels. Biosci Rep. 2004; 24:127–163. [PubMed: 16209125]

Altenbach C, Greenhalgh DA, Khorana HG, Hubbell WL. A collision gradient method to determine the immersion depth of nitroxides in lipid bilayers: application to spin-labeled mutants of bacteriorhodopsin. Proc Natl Acad Sci U S A. 1994; 91:1667–1671. [PubMed: 8127863]

Ashikawa I, Yin JJ, Subczynski WK, Kouyama T, Hyde JS, Kusumi A. Molecular organization and dynamics in bacteriorhodopsin-rich reconstituted membranes: discrimination of lipid environments by the oxygen transport parameter using a pulse ESR spin-labeling technique. Biochemistry. 1994; 33:4947–4952. [PubMed: 8161556]

Bassnett S, Shi Y, Vrensen GF. Biological glass: structural determinants of eye lens transparency. Philos Trans Royal Soc Lond Ser B Biol Sci. 2011; 366:1250–1264.

Beebe, DC. The lens. In: Kaufman, PL., editor. Physiology of the eye. Mosby-Year Book; St Louis: 2003. p. 117-158.

Beebe DC, Holekamp NM, Siegfried C, Shui YB. Vitreoretinal influences on lens function and cataract. Philos Trans Royal Soc Lond Ser B Biol Sci. 2011; 366:1293–1300.

Beebe DC, Shui YB, Siegfried CJ, Holekamp NM, Bai F. Preserve the (intraocular) environment: the importance of maintaining normal oxygen gradients in the eye. Jap J Ophthalmol. 2014; 58:225–231. [PubMed: 24687817]

Bieri VG, Wallach DF. Variations of lipid-protein interactions in erythrocyte ghosts as a function of temperature and pH in physiological and non-physiological ranges. A study using a paramagnetic

quenching of protein fluorescence by nitroxide lipid analogues. Biochim Biophys Acta. 1975; 406:415–423. [PubMed: 241415]

Biswas SK, Lo WK. Gap junctions contain different amounts of cholesterol which undergo unique sequestering processes during fiber cell differentiation in the embryonic chicken lens. Mol Vis. 2007; 13:345–359. [PubMed: 17392685]

Biswas SK, Jiang JX, Lo WK. Gap junction remodeling associated with cholesterol redistribution during fiber cell maturation in the adult chicken lens. Mol Vis. 2009; 15:1492–1508. [PubMed: 19657477]

Biswas SK, Lee JE, Brako L, Jiang JX, Lo WK. Gap junctions are selectively associated with interlocking ball-and-sockets but not protrusions in the lens. Mol Vis. 2010; 16:2328–2341. [PubMed: 21139982]

Bloemendal H, Zweers A, Vermorken F, Dunia I, Benedetti EL. The plasma membranes of eye lens fibres. Biochemical and structural characterization. Cell Differ. 1972; 1:91–106. [PubMed: 4275925]

Borchman D, Byrdwell WC, Yappert MC. Regional and age-dependent differences in the phospholipid composition of human lens membranes. Invest Ophthalmol Vis Sci. 1994; 35:3938–3942. [PubMed: 7928192]

Borchman D, Giblin FJ, Leverenz VR, Reddy VN, Lin LR, Yappert MC, Tang D, Li L. Impact of aging and hyperbaric oxygen in vivo on guinea pig lens lipids and nuclear light scatter. Invest Ophthalmol Vis Sci. 2000; 41:3061–3073. [PubMed: 10967065]

Borchman D, Yappert MC. Lipids and the ocular lens. J Lipid Res. 2010; 51:2473–2488. [PubMed: 20407021]

Bron AJ, Vrensen GF, Koretz J, Maraini G, Harding JJ. The ageing lens. Ophthalmologica. 2000; 214:86–104. [PubMed: 10657747]

Buzhynskyy N, Hite RK, Walz T, Scheuring S. The supramolecular architecture of junctional microdomains in native lens membranes. EMBO Rep. 2007; 8:51–55. [PubMed: 17124511]

Buzhynskyy N, Sens P, Behar-Cohen F, Scheuring S. Eye lens membrane junctional microdomains: a comparison between healthy and pathologicalcases. New J Phys. 2011; 13:1–16.

Cenedella RJ, Fleschner CR. Selective association of crystallins with lens ‘native’ membrane during dynamic cataractogenesis. Curr Eye Res. 1992; 11:801–815. [PubMed: 1424724]

Chandrasekher G, Cenedella RJ. Protein associated with human lens ‘native’ membrane during aging and cataract formation. Exp Eye Res. 1995; 60:707–717. [PubMed: 7641853]

Chung CP, Hsu SY, Wu WC. Cataract formation after pars plana vitrectomy. Kaoh J Med Sci. 2001; 17:84–89.

Chung J, Berthoud VM, Novak L, Zoltoski R, Heilbrunn B, Minogue PJ, Liu X, Ebihara L, Kuszak J, Beyer EC. Transgenic overexpression of connexin50 induces cataracts. Exp Eye Res. 2007; 84:513–528. [PubMed: 17217947]

Costello MJ, McIntosh TJ, Robertson JD. Distribution of gap junctions and square array junctions in the mammalian lens. Invest Ophthalmol Vis Sci. 1989; 30:975–989. [PubMed: 2722452]

Deeley JM, Mitchell TW, Wei X, Korth J, Nealon JR, Blanksby SJ, Truscott RJ. Human lens lipids differ markedly from those of commonly used experimental animals. Biochim Biophys Acta. 2008; 1781:288–298. [PubMed: 18474264]

Dunia I, Cibert C, Gong X, Xia CH, Recouvreur M, Levy E, Kumar N, Bloemendal H, Benedetti EL. Structural and immunocytochemical alterations in eye lens fiber cells from Cx46 and Cx50 knockout mice. Eur J Cell Biol. 2006; 85:729–752. [PubMed: 16740340]

Eaton JW. Is the lens canned? Free Radic Biol Med. 1991; 11:207–213. [PubMed: 1937139]

Epand, RM. Role of membrane lipids in modulating the activity of membrane-bound enzymes. In: Yeagle, PL., editor. The Structure of Biological Membrane. CRC Press; Boca Raton: 2005. p. 499-509.

Estrada R, Puppato A, Borchman D, Yappert MC. Reevaluation of the phospholipid composition in membranes of adult human lenses by (31)P NMR and MALDI MS. Biochim Biophys Acta. 2010; 1798:303–311. [PubMed: 19925778]

Estrada R, Yappert MC. Regional phospholipid analysis of porcine lens membranes by matrix-assisted laser desorption/ionization time-of-flight mass spectrometry. J Mass Spectrom. 2004; 39:1531–1540. [PubMed: 15578747]

Freel CD, Gilliland KO, Mekeel HE, Giblin FJ, Costello MJ. Ultrastructural characterization and Fourier analysis of fiber cell cytoplasm in the hyperbaric oxygen treated guinea pig lens opacification model. Exp Eye Res. 2003; 76:405–415. [PubMed: 12634105]

Gonen T, Cheng Y, Kistler J, Walz T. Aquaporin-0 membrane junctions form upon proteolytic cleavage. J Mol Biol. 2004; 342:1337–1345. [PubMed: 15351655]

Gonen T, Cheng Y, Sliz P, Hiroaki Y, Fujiyoshi Y, Harrison SC, Walz T. Lipid-protein interactions in double-layered two-dimensional AQP0 crystals. Nature. 2005; 438:633–638. [PubMed: 16319884]

Harding, JJ. Cataract, biochemistry, epidemiology and pharmacology. Chapman and Hall; London: 1991.

Harocopos GJ, Shui YB, McKinnon M, Holekamp NM, Gordon MO, Beebe DC. Importance of vitreous liquefaction in age-related cataract. Invest Ophthalmol Vis Sci. 2004; 45:77–85. [PubMed: 14691157]

Hsuan JD, Brown NA, Bron AJ, Patel CK, Rosen PH. Posterior subcapsular and nuclear cataract after vitrectomy. J Cataract Refract Surg. 2001; 27:437–444. [PubMed: 11255058]

Huang L, Estrada R, Yappert MC, Borchman D. Oxidation-induced changes in human lens epithelial cells. 1 Phospholipids. Free Radic Biol Med. 2006; 41:1425–1432. [PubMed: 17023269]

Huang L, Yappert MC, Jumblatt MM, Borchman D. Hyperoxia and thyroxine treatment and the relationships between reactive oxygen species generation, mitochondrial membrane potential, and cardiolipin in human lens epithelial cell cultures. Curr Eye Res. 2008; 33:575–586. [PubMed: 18600490]

Jacob RF, Cenedella RJ, Mason RP. Direct evidence for immiscible cholesterol domains in human ocular lens fiber cell plasma membranes. J Biol Chem. 1999; 274:31613–31618. [PubMed: 10531368]

Kawasaki K, Yin JJ, Subczynski WK, Hyde JS, Kusumi A. Pulse EPR detection of lipid exchange between protein rich raft and bulk domains in the membrane: methodology development and its application to studies of influenza viral membrane. Biophys J. 2001; 80:738–748. [PubMed: 11159441]

Kistler J, Bullivant S. Lens gap junctions and orthogonal arrays are unrelated. FEBS Lett. 1980; 111:73–78. [PubMed: 7358167]

Kusumi A, Subczynski WK, Hyde JS. Oxygen transport parameter in membranes as deduced by saturation recovery measurements of spin-lattice relaxation times of spin labels. Proc Natl Acad Sci U S A. 1982; 79:1854–1858. [PubMed: 6952236]

Kuszak JR, Zoltoski RK, Tiedemann CE. Development of lens sutures. Int J Dev Biol. 2004; 48:889–902. [PubMed: 15558480]

Li LK, Roy D, Spector A. Changes in lens protein in concentric fractions from individual normal human lenses. Curr Eye Res. 1986; 5:127–135. [PubMed: 3956240]

Li LK, So L, Spector A. Membrane cholesterol and phospholipid in consecutive concentric sections of human lenses. J Lipid Res. 1985; 26:600–609. [PubMed: 4020298]

Li LK, So L, Spector A. Age-dependent changes in the distribution and concentration of human lens cholesterol and phospholipids. Biochim Biophys Acta. 1987; 917:112–120. [PubMed: 3790601]

Ligeza A, Tikhonov AN, Hyde JS, Subczynski WK. Oxygen permeability of thylakoid membranes: electron paramagnetic resonance spin labeling study. Biochim Biophys Acta. 1998; 1365:453–463. [PubMed: 9711298]

Lim J, Lam YC, Kistler J, Donaldson PJ. Molecular characterization of the cystine/glutamate exchanger and the excitatory amino acid transporters in the rat lens. Invest Ophthalmol Vis Sci. 2005; 46:2869–2877. [PubMed: 16043861]

Lynnerup N, Kjeldsen H, Heegaard S, Jacobsen C, Heinemeier J. Radiocarbon dating of the human eye lens crystallines reveal proteins without carbon turnover throughout life. PLoS One. 2008; 3:e1529. [PubMed: 18231610]

Mailer C, Nielsen RD, Robinson BH. Explanation of spin-lattice relaxation rates of spin labels obtained with multifrequency saturation recovery EPR. J Phys Chem A. 2005; 109:4049–4061. [PubMed: 16833727]

Mainali L, Feix JB, Hyde JS, Subczynski WK. Membrane fluidity profiles as deduced by saturation-recovery EPR measurements of spin-lattice relaxation times of spin labels. J Magn Reson. 2011a; 212:418–425. [PubMed: 21868272]

Mainali L, Hyde JS, Subczynski WK. Using spin-label W-band EPR to study membrane fluidity profiles in samples of small volume. J Magn Reson. 2013a; 226:35–44. [PubMed: 23207176]

Mainali L, Raguz M, Camenisch TG, Hyde JS, Subczynski WK. Spin-label saturation-recovery EPR at W-band: applications to eye lens lipid membranes. J Magn Reson. 2011b; 212:86–94. [PubMed: 21745756]

Mainali L, Raguz M, O'Brien WJ, Subczynski WK. Properties of fiber cell plasma membranes isolated from the cortex and nucleus of the porcine eye lens. Exp Eye Res. 2012; 97:117–129. [PubMed: 22326289]

Mainali L, Raguz M, O'Brien WJ, Subczynski WK. Properties of membranes derived from the total lipids extracted from the human lens cortex and nucleus. Biochim Biophys Acta. 2013b; 1828:1432–1440. [PubMed: 23438364]

Mainali L, Raguz M, O'Brien WJ, Subczynski WK. Properties of membranes derived from the total lipids extracted from clear and cataractous lenses of 61–70-year-old human donors. Eur Biophys. 201510.1007/s00249014-1004-7

Mathias RT, White TW, Gong X. Lens gap junctions in growth, differentiation, and homeostasis. Physiol Rev. 2010; 90:179–206. [PubMed: 20086076]

McNulty R, Wang H, Mathias RT, Ortwerth BJ, Truscott RJ, Bassnett S. Regulation of tissue oxygen levels in the mammalian lens. J Physiol. 2004; 559:883–898. [PubMed: 15272034]

Palmquist BM, Philipson B, Barr PO. Nuclear cataract and myopia during hyperbaric oxygen therapy. Br J Ophthalmol. 1984; 68:113–117. [PubMed: 6691953]

Rafferty, NS. Lens morphology. In: Maisel, H., editor. The ocular lens:structure, function and pathology. Marcel Dekker; New York: 1985. p. 1-60.

Raguz M, Mainali L, O'Brien WJ, Subczynski WK. Lipid-protein interactions in plasma membranes of fiber cells isolated from the human eye lens. Exp Eye Res. 2014; 120:138–151. [PubMed: 24486794]

Raguz M, Mainali L, Widomska J, Subczynski WK. The immiscible cholesterol bilayer domain exists as an integral part of phospholipid bilayer membranes. Biochim Biophys Acta. 2011a; 1808:1072–1080. [PubMed: 21192917]

Raguz M, Mainali L, Widomska J, Subczynski WK. Using spin-label electron paramagnetic resonance (EPR) to discriminate and characterize the cholesterol bilayer domain. Chem Phys Lipids. 2011b; 164:819–829. [PubMed: 21855534]

Raguz M, Widomska J, Dillon J, Gaillard ER, Subczynski WK. Characterization of lipid domains in reconstituted porcine lens membranes using EPR spin-labeling approaches. Biochim Biophys Acta. 2008; 1778:1079–1090. [PubMed: 18298944]

Raguz M, Widomska J, Dillon J, Gaillard ER, Subczynski WK. Physical properties of the lipid bilayer membrane made of cortical and nuclear bovine lens lipids: EPR spin-labeling studies. Biochim Biophys Acta. 2009; 1788:2380–2388. [PubMed: 19761756]

Reichow SL, Gonen T. Lipid-protein interactions probed by electron crystallography. Curr Opin Struct Biol. 2009; 19:560–565. [PubMed: 19679462]

Robinson BH, Haas DA, Mailer C. Molecular dynamics in liquids: spin-lattice relaxation of nitroxide spin labels. Science. 1994; 263:490–493. [PubMed: 8290958]

Rujoi M, Jin J, Borchman D, Tang D, Yappert MC. Isolation and lipid characterization of cholesterol-enriched fractions in cortical and nuclear human lens fibers. Invest Ophthalmol Vis Sci. 2003; 44:1634–1642. [PubMed: 12657603]

Ryba NJ, Horvath LI, Watts A, Marsh D. Molecular exchange at the lipid-rhodopsin interface: spin-label electron spin resonance studies of rhodopsin-dimyristoylphosphatidylcholine recombinants. Biochemistry. 1987; 26:3234–3240. [PubMed: 3038180]

Siegfried CJ, Shui YB, Holekamp NM, Bai F, Beebe DC. Oxygen distribution in the human eye: relevance to the etiology of open-angle glaucoma after vitrectomy. Invest Ophthalmol Vis Sci. 2010; 51:5731–5738. [PubMed: 20720218]

Subczynski WK, Felix CC, Klug CS, Hyde JS. Concentration by centrifugation for gas exchange EPR oximetry measurements with loop-gap resonators. J Magn Reson. 2005; 176:244–248. [PubMed: 16040261]

Subczynski WK, Hopwood LE, Hyde JS. Is the mammalian cell plasma membrane a barrier to oxygen transport? J Gen Physiol. 1992a; 100:69–87. [PubMed: 1324973]

Subczynski WK, Hyde JS, Kusumi A. Oxygen permeability of phosphatidylcholine-cholesterol membranes. Proc Natl Acad Sci U S A. 1989; 86:4474–4478. [PubMed: 2543978]

Subczynski WK, Raguz M, Widomska J, Mainali L, Konovalov A. Functions of cholesterol and the cholesterol bilayer domain specific to the fiber-cell plasma membrane of the eye lens. J Membr Biol. 2012; 245:51–68. [PubMed: 22207480]

Subczynski WK, Renk GE, Crouch RK, Hyde JS, Kusumi A. Oxygen diffusion-concentration product in rhodopsin as observed by a pulse ESR spin labeling method. Biophys J. 1992b; 63:573–577. [PubMed: 1330032]

Subczynski, WK.; Widomska, J.; Wisniewska, A.; Kusumi, A. Saturation-recovery electron paramagnetic resonance discrimination by oxygen transport (DOT) method for characterizing membrane domains. In: McIntosh, TJ., editor. Methods in Molecular Biology, Lipid Rafts. Humana Press; Totowa: 2007. p. 143-157.

Subczynski WK, Wisniewska A, Yin JJ, Hyde JS, Kusumi A. Hydrophobic barriers of lipid bilayer membranes formed by reduction of water penetration by alkyl chain unsaturation and cholesterol. Biochemistry. 1994; 33:7670–7681. [PubMed: 8011634]

Tenbroek E, Arneson M, Jarvis L, Louis C. The distribution of the fiber cell intrinsic membrane proteins MP20 and connexin46 in the bovine lens. J Cell Sci. 1992; 103:245–257. [PubMed: 1331134]

Tong J, Briggs Margaret M, McIntosh Thomas J. Water Permeability of Aquaporin-4 Channel Depends on Bilayer Composition, Thickness, and Elasticity. Biophys J. 2012; 103:1899–1908. [PubMed: 23199918]

Tong J, Canty JT, Briggs MM, McIntosh TJ. The water permeability of lens aquaporin-0 depends on its lipid bilayer environment. Exp Eye Res. 2013; 113:32–40. [PubMed: 23680159]

Truscott RJ. Age-related nuclear cataract-oxidation is the key. Exp Eye Res. 2005; 80:709–725. [PubMed: 15862178]

Warren GB, Houslay MD, Metcalfe JC, Birdsall NJ. Cholesterol is excluded from the phospholipid annulus surrounding an active calcium transport protein. Nature. 1975; 255:684–687. [PubMed: 124402]

White TW, Goodenough DA, Paul DL. Targeted ablation of connexin50 in mice results in microphthalmia and zonular pulverulent cataracts. J Cell Bio. 1998; 143:815–825. [PubMed: 9813099]

Widomska J, Raguz M, Dillon J, Gaillard ER, Subczynski WK. Physical properties of the lipid bilayer membrane made of calf lens lipids: EPR spin labeling studies. Biochim Biophys Acta. 2007a; 1768:1454–1465. [PubMed: 17451639]

Widomska J, Raguz M, Subczynski WK. Oxygen permeability of the lipid bilayer membrane made of calf lens lipids. Biochim Biophys Acta. 2007b; 1768:2635–2645. [PubMed: 17662231]

Wride MA. Lens fibre cell differentiation and organelle loss: many paths lead to clarity. Philos Trans Royal Soc Lond Ser B Biol Sci. 2011; 366:1219–1233.

Yappert MC, Borchman D. Sphingolipids in human lens membranes: an update on their composition and possible biological implications. Chem Phys Lipids. 2004; 129:1–20. [PubMed: 14998723]

Yappert MC, Rujoi M, Borchman D, Vorobyov I, Estrada R. Glycero- versus sphingo-phospholipids: correlations with human and non-human mammalian lens growth. Exp Eye Res. 2003; 76:725–734. [PubMed: 12742355]

Yin JJ, Subczynski WK. Effects of lutein and cholesterol on alkyl chain bending in lipid bilayers: a pulse electron spin resonance spin labeling study. Biophys J. 1996; 71:832–839. [PubMed: 8842221]

Zampighi GA, Eskandari S, Hall JE, Zampighi L, Kreman M. Micro-domains of AQP0 in lens equatorial fibers. Exp Eye Res. 2002; 75:505–519. [PubMed: 12457863]

Zelenka PS. Lens lipids. Curr Eye Res. 1984; 3:1337–1359. [PubMed: 6391828]

- Results show changes in the organization of lens membrane lipids that occur with age
- Three distinct lipid environments were identified: bulk, boundary, and trapped lipids
- Amount of boundary and trapped lipids was greater in nucleus than in cortex
- Amount of boundary and trapped lipids in nuclear membranes increased with the age

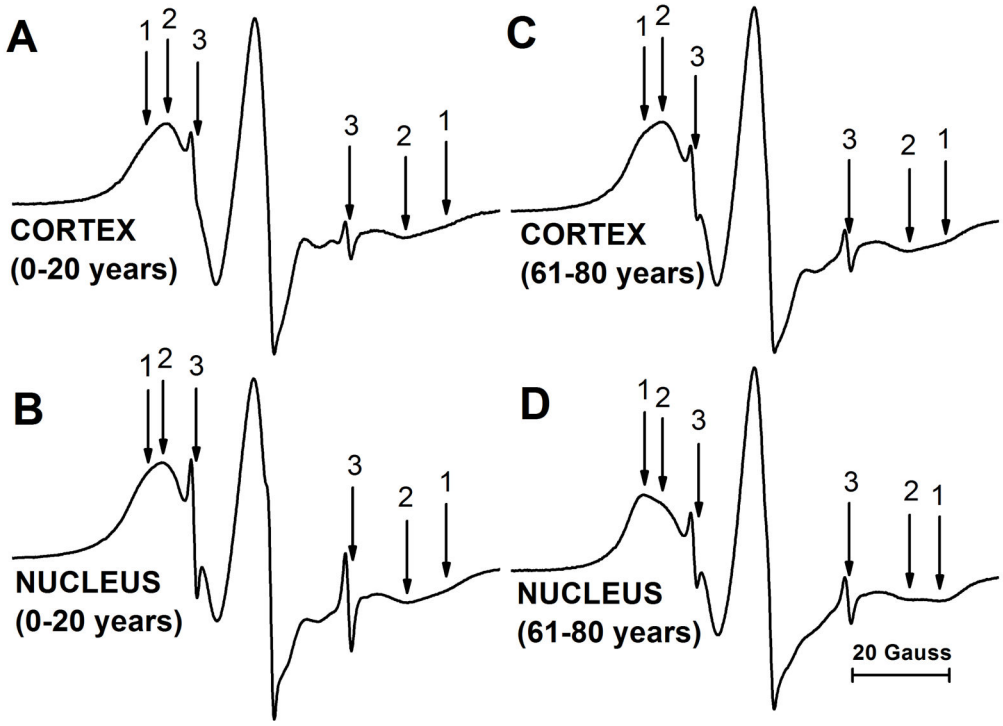

Fig. 1.

Representative EPR spectra of 12-SASL from cortical (A,C) and nuclear (B,D) intact membranes from clear human lenses of 0 to 20 (A,B) and 61 to 80 (C,D) year old donors. Spectra were recorded at 37°C. Arrows 1–3 represent spectra from strongly immobilized, weakly immobilized, and water components, respectively. The positions of certain peaks were evaluated with a high level of precision by monitoring them at 10 times higher receiver gain and, when necessary, a higher modulation amplitude.

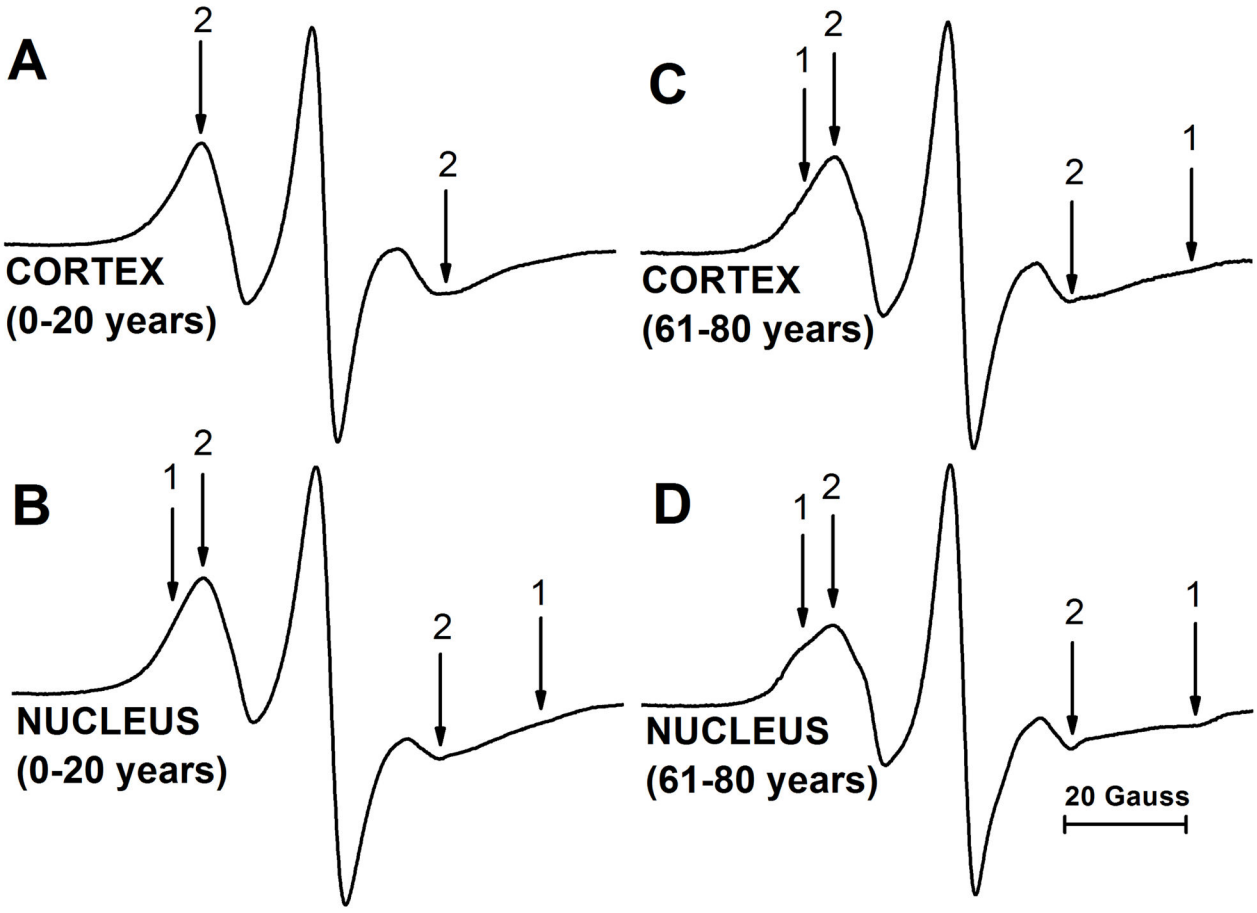

Fig. 2.

Representative EPR spectra of ASL from cortical (A,C) and nuclear (B,D) intact membranes from clear human lenses of 0 to 20 (A,B) and 61 to 80 (C,D) year old donors. Spectra were recorded at 37°C. Arrows 1 and 2 represent spectra from strongly immobilized and weakly immobilized components, respectively. The positions of certain peaks were evaluated with a high level of precision by monitoring them at 10 times higher receiver gain and, when necessary, a higher modulation amplitude.

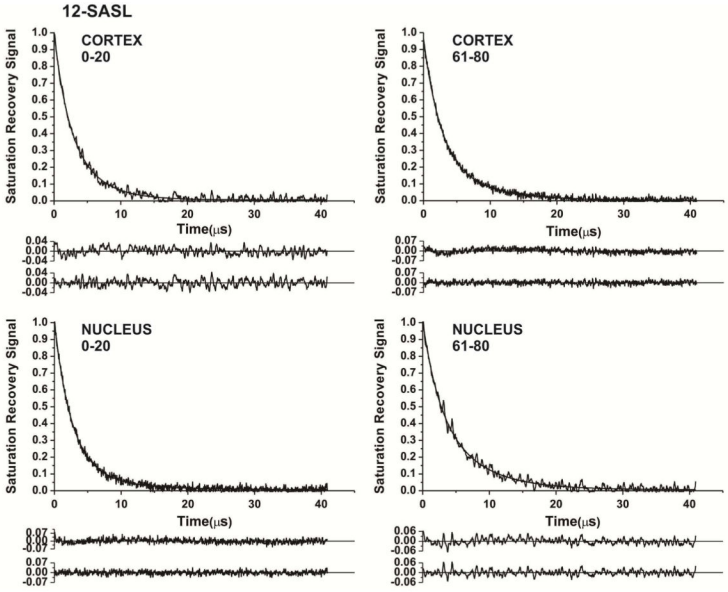

Fig. 3.

Representative SR signals with fitted curves and residuals (the experimental signal minus the fitted curve) of 12-SASL from cortical (A.C) and nuclear (B,D) intact membranes from clear human lenses of 0 to 20 (A,B) and 61 to 80 (C,D) year old donors. Signals were recorded at 37°C for deoxygenated samples (equilibrated with 100% nitrogen). The SR signals can be satisfactorily fitted with only a double-exponential function with time constants of 4.27 ± 0.70 μs and 1.90 ± 0.60 μs (A), 6.0 ± 0.8 μs and 2.41 ± 0.1 μs (B), 7.22 ± 0.60 μs and 2.59 ± 0.10 μs (C), and 6.22 ± 0.80 μs and 2.35 ± 0.5 μs (D). The first residuals are for single- and the second residuals for double-exponential fits.

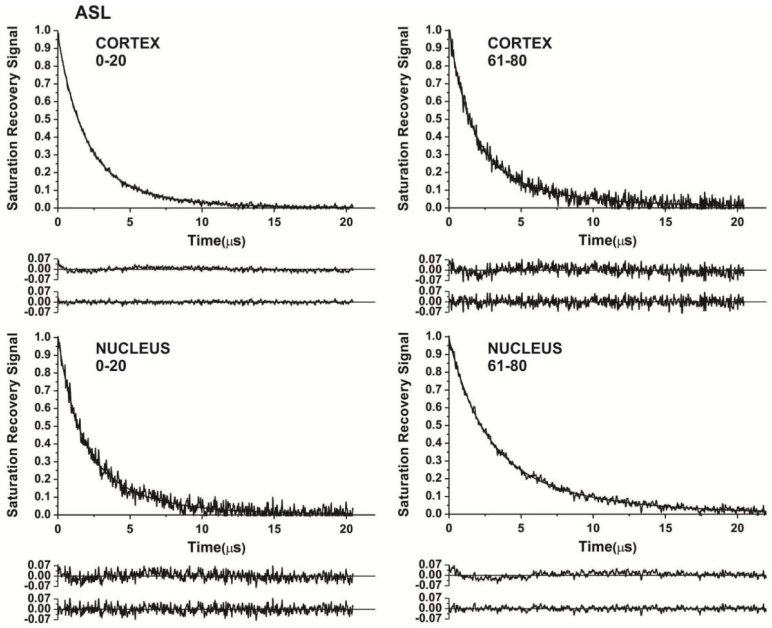

Fig. 4.

Representative SR signals with fitted curves and residuals (the experimental signal minus the fitted curve) of ASL from cortical (A.C) and nuclear (B,D) intact membranes from clear human lenses of 0 to 20 (A,B) and 61 to 80 (C,D) year old donors.. Signals were recorded at 37°C for deoxygenated samples (equilibrated with 100% nitrogen). The SR signals can be satisfactorily fitted with only a double-exponential function with time constants of 4.03 ± 0.20 μs and 1.56 ± 0.10 μs (A), 3.81 ± 0.30 μs and 1.23 ± 0.10 μs (B), 4.66 ± 0.50 μs and 1.40 ± 0.10 μs (C), and 6.43 ± 0.30 μs and 2.18 ± 0.10 μs (D). The first residuals are for single- and the second residuals for double-exponential fits.

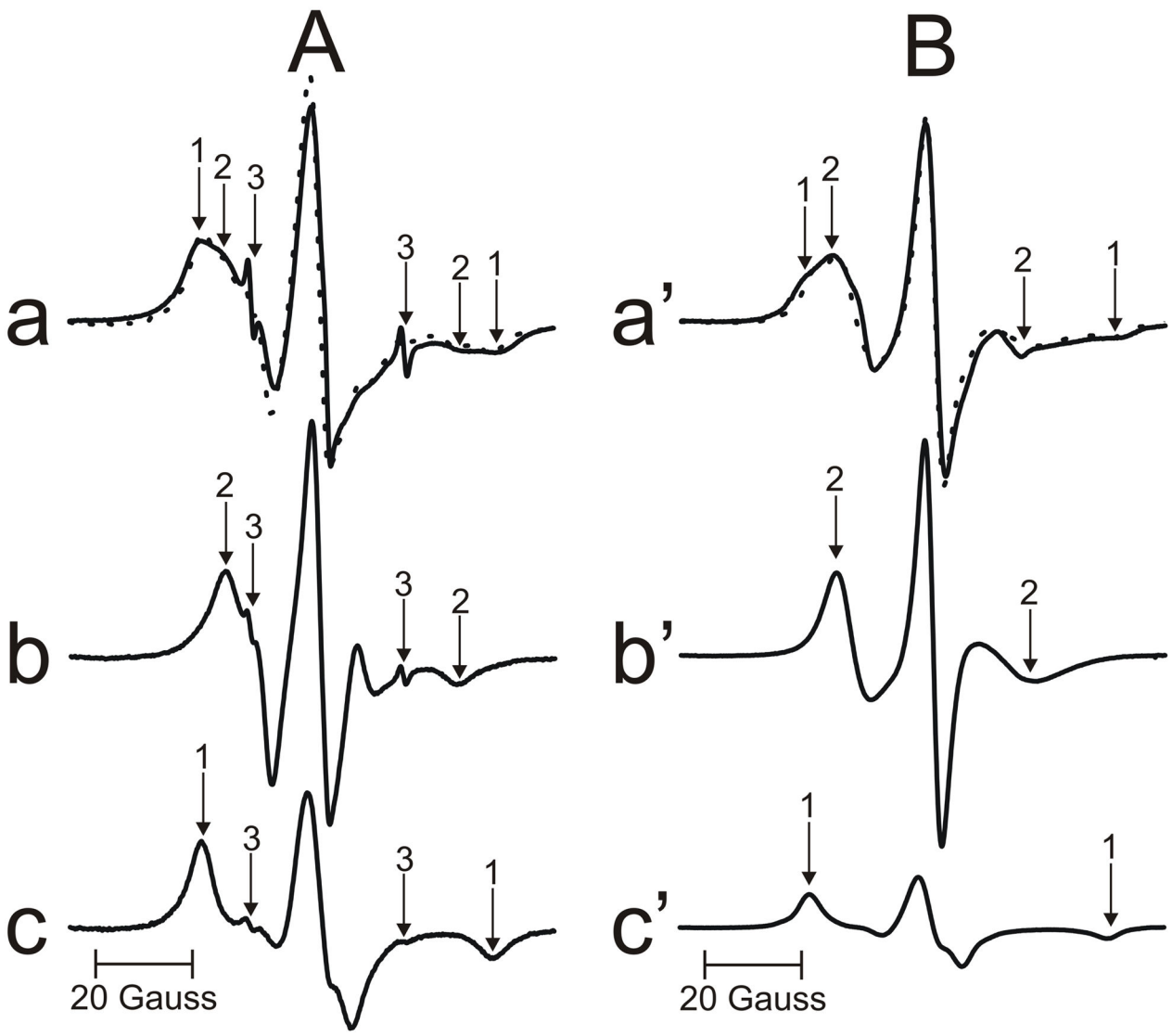

Fig. 5.

(A) The procedure for the evaluation of the relative amount of PLs in domains in the lipid bilayer portion of intact membrane is illustrated based on the EPR spectrum of 12-SASL in nuclear membranes from clear human lenses of 61 to 80 year old donors. The EPR spectrum of 12-SASL in the nuclear intact membranes obtained at 37°C (a – solid line). The EPR spectrum of 12-SASL in nuclear lens lipid membranes obtained at 37°C (b). The EPR spectrum of 12-SASL in nuclear lens lipid membranes obtained at −10°C (c) (this spectrum has the same maximum splitting as the strongly immobilized component in spectrum (a)). The dotted spectrum (a) was obtained by adding 44% of spectrum (b) and 56% of spectrum (c). Arrows 1–3 represent spectra from strongly immobilized, weakly immobilized, and water components, respectively. (B) The procedure for the evaluation of the relative amount of Chol in domains in the lipid bilayer portion of intact membrane is illustrated based on the EPR spectrum of ASL in nuclear membranes from clear human lenses of 61 to 80 year old donors. The EPR spectrum of ASL in the nuclear intact membranes obtained at 37°C (a′ –

solid line). The EPR spectrum of ASL in nuclear lens lipid membranes obtained at 37°C (b ′). The EPR spectrum of ASL in nuclear lens lipid membranes obtained at −13°C (c′) (this spectrum has the same maximum splitting as the strongly immobilized component in spectrum (a)). The dotted spectrum (a′) was obtained by adding 40% of spectrum (b′) and 60% of spectrum (c′). Arrows 1 and 2 represent spectra from strongly immobilized and weakly immobilized components, respectively.

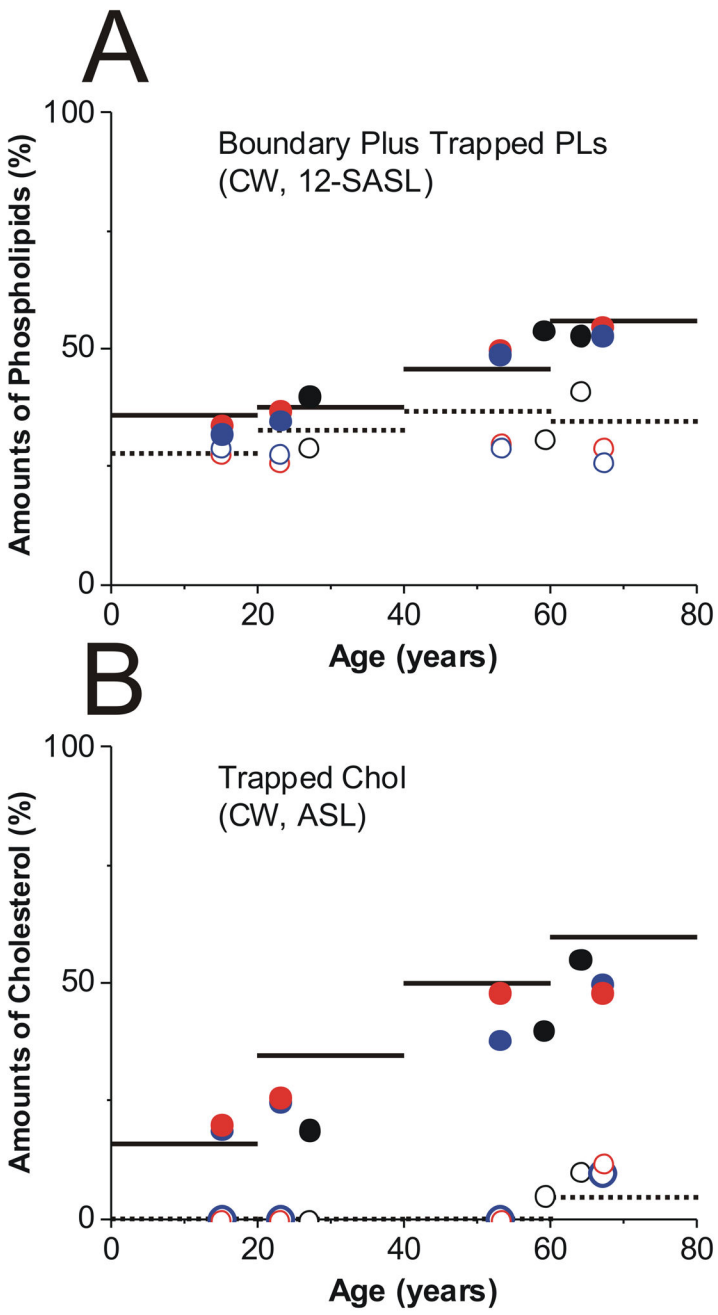

Fig. 6.

Amounts of PLs (A, % of total PLs) and Chol (B, % of total Chol) in domains uniquely formed due to the presence of membrane proteins in human intact cortical (·····) and nuclear (——) lens membranes. Data were obtained for samples from pools of ~20 clear lenses from donors of three age groups (0 – 20, 21 – 40, and 61 – 80). Data for the age group 41 – 60 were taken from our recent publication (Raguz et al., 2014). A – results obtained based on conventional (CW) EPR spectra of 12-SASL (as indicated in Fig. 5A). B – results obtained based on conventional (CW) EPR spectra of ASL (as indicated in Fig. 5B). Data obtained

for single donors (●, ○) and single lenses ((●, ○) right and (●, ○) left eye lens of the same donor) are included. Filled symbols are for nuclear and open for cortical membranes.

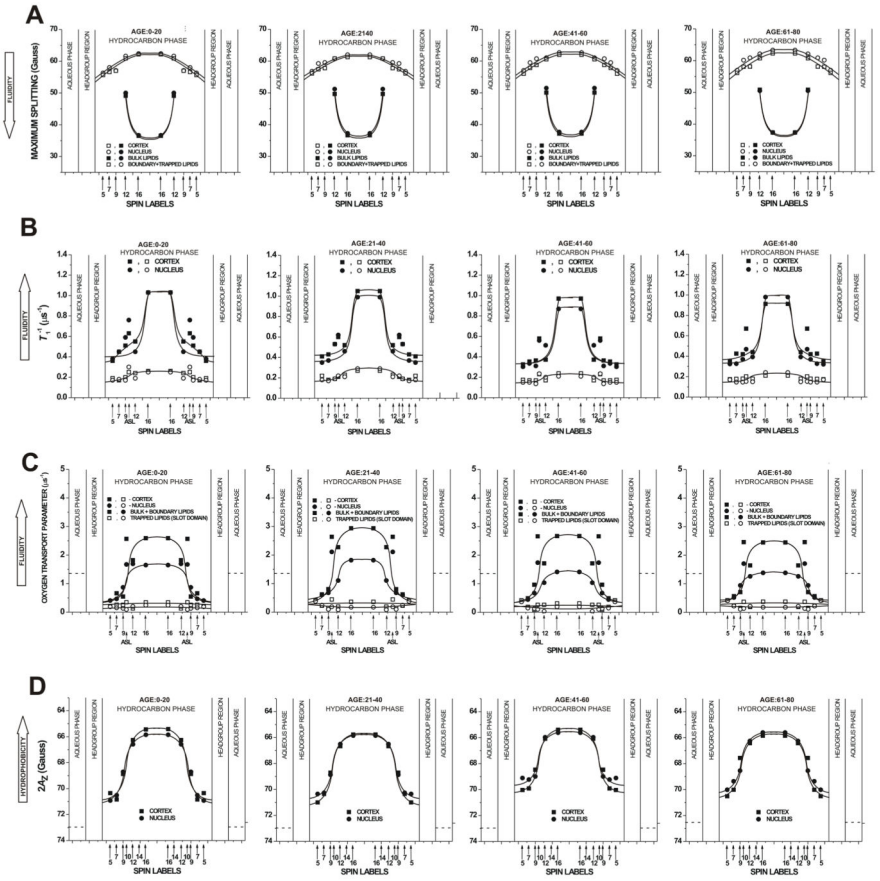

Fig. 7.

Profiles of the maximum splitting (A), T_1^{-1} (the spin-lattice relaxation rate) (B), OTP (C), and hydrophobicity ($2A_Z$) (D) across domains in intact cortical and nuclear fiber-cell plasma membranes. Profiles were obtained for samples from pools of ~20 clear lenses from donors of three age groups (0 – 20 years, 21 – 40 years, and 61 – 80 years). Profiles for the age group 41 – 60 years were taken from our recent publication (Raguz et al., 2014), except those in (B) for which T_1^{-1} values were evaluated again based on the same procedure as for other age groups.

Table 1

Amounts of PLs (% of total PLs) and Chol (% of total Chol) in domains uniquely formed due to the presence of membrane proteins in human intact lens membranes from single donor and single lens preparations. Mean values and standard deviations for donors grouped around the average age of 20.6 (age group from 15 to 27) and 60.5 (age group from 53 to 67) years (see Fig. 6 for individual data) are presented.

	Boundary + Trapped PLs		**Trapped Chol**	
Average age (years)	20.6	60.5	20.6	60.5
Nucleus	35.6 ± 3.0	52.3 ± 2.3	21.8 ± 3.42	46.5 ± 6.4
Cortex	30.2 ± 5.6	31.0 ± 5.2	0 ± 5[a]	6.2 ± 5.3
Nucleus -Cortex	5.4 ± 4.2	21.3 ± 5.4	21.8 ± 3.4	40.3 ± 5.2

[a]Precision of the individual measurement instead of the standard deviation is indicated.

P values determined by Student's *t* test indicated that; in nuclear membranes the amount of boundary + trapped PLs at the donor age of 60.5 was greater than that at age of 20.6 with $P < 0.001$ and in cortical membranes with $P = 0.4$, in nuclear membranes the amount of trapped Chol at the donor age of 60.5 was greater than that at age of 20.6 with $P < 0.001$ and in cortical membranes with $P = 0.04$, at the donor age of 20.6 the amount of boundary + trapped PLs was greater in nuclear than in cortical membranes with $P = 0.054$ and the amount of trapped Chol with $P = 0.001$, at the donor age of 60.5 the amount of boundary + trapped PLs was greater in nuclear than in cortical membranes with $P < 0.001$ and the amount of Chol with $P < 0.001$, the difference of boundary + trapped PLs between nuclear and cortical membranes increases with the age (between average donor age of 20.6 and 60.5) with $P < 0.001$ and the difference of trapped Chol with $P < 0.001$.

Table 2

Permeability coefficients for oxygen, P_M (cm/s), across the hydrocarbon region of domains in human intact membranes of different age groups at 37 °C

	Age Group			
	0–21	**21–40**	**41–60**[b]	**61–80**
Cortical intact membranes (bulk + boundary lipids)	76.9±23[c]	79.8±24	66.3 ±20	73.2±22
Nuclear intact membranes (bulk + boundary lipids)	51.7±15	45.0±13	53.8 ±16	50.7±15
Cortical intact membranes (trapped lipids)	19.1±6	23.1±7	16.8 ±5.0	23.2±7
Nuclear intact membranes (trapped lipids)	12.8±4	10.2±3	8.5 ±2.5	13.9±4
Water layer[a]	94.4±28	94.4±28	94.4 ±28	94.4±28

[a] The thickness of the water layer is the same as the hydrocarbon region.

[b] Data taken from Raguz et al., 2014.

[c] P_M was determined as the mean of the maximal and the minimal evaluation, which takes the uncertainty of the location of the spin label nitroxide group into account (Subczynski et al., 1989; Widomska et al., 2007b). Mean values ± differences between mean values and maximal (minimal) evaluations are indicated.